

Discrete-Time Dynamics of Molecular Ground State with a Double Similarity Transformed Coupled Cluster Theory

Valay Agarawal, Anish Chakraborty, and Rahul Maitra*

Department of Chemistry, Indian Institute of Technology Bombay, Powai, Mumbai 400076, India

The discrete-time propagation of a double similarity transformed Coupled Cluster theory with input perturbation is studied. The coupled iterative scheme to solve the ground state Schrödinger equation is cast as a multivariate logistic map, the solutions show the universal Feigenbaum dynamics. Using recurrence analysis, it is shown that the dynamics is dictated by a small subgroup of cluster operators, mostly those involving chemically active orbitals, whereas all other cluster operators with smaller amplitudes are enslaved.

Introduction and Theory: Coupled Cluster (CC) theory[1–4] is an accurate electronic structure methodology to compute the energetics and properties of small to medium-sized atoms and molecules. CC theory, with singles, doubles, and perturbative triples excitations—the so-called CCSD(T)[5–7]—is known to provide very accurate results for molecules in their near-equilibrium geometry. Recently, a new iterative scheme, which takes care of the fully connected triple excitations at a computational cost less than that of CCSD(T). The said method, known as the *iterative n-body excitation inclusive CCSD*, (*iCCSDn*)[8, 9] parametrizes the wavefunction as a double exponential waveoperator Ω acting on a reference zeroth-order wavefunction, usually taken to be the Hartree-Fock (HF) determinant.

$$\Omega = \{\exp(S)\} \exp(T_1 + T_2) \quad (1)$$

where T 's are the usual CCSD excitation operators (*aka* cluster operators), and S denote scattering operators that induce higher excitations by their action on the doubly excited determinants. S and T operators do not commute. The presence of hole→hole (or particle→particle) scattering in S ensures that its action on HF determinant is trivially zero, but not on an excited determinant. The higher rank correlation effect is simulated via the contraction of S and T operators, and hence it provides the accuracy at a cheap computational scaling. The quantity inside $\{\dots\}$ denotes 'Normal Ordering,' which ensures the CC expansion terminates at finite power. The effective Hamiltonian, G , is constructed via two similarity transformations recursively.

$$G = e^{-(T_1+T_2)} W e^{(T_1+T_2)} \quad (2)$$

where, $W = \overbrace{\{H \exp(S) - (\exp(S) - 1)H \exp(S)\}}^{\text{Wick contraction}}$ is the first similarity transformed Hamiltonian obtained through the time-independent Wick's theorem and the connections depict Wick contraction. The determination of the cluster operators can be done in a coupled manner at a scaling marginally higher than CCSD. The cluster operator T 's are responsible for inducing the dynamical correlation, whereas the S operators renormalize them

through a set of local denominators, by including the effects of connected triple excitations within the two-body cluster amplitudes. Thus, they are expected to be large at stretched molecular geometries. Note that the S operators do not have any direct effect on energy; however they do indirectly contribute at high perturbative orders by renormalizing the cluster amplitudes.

Following a many-body expansion[10] of the double similarity transformed Hamiltonian, G , the amplitudes $t(s)$ associated with $T(S)$ and operators are obtained through a set of coupled non-linear equations by demanding $g_\mu = g_\alpha = 0$ upon convergence. Here g is the amplitude associated with the tensor G and μ (α) are the collective orbital labels associated with the tensor T (S). Let us denote the orbital labels associated with T as μ, ν, \dots , etc. and those associated with the scattering operator S as α, β, \dots etc. In the iteration procedure, the discrete-time propagation of vector at $(n+1)$ -th step can be represented as logistic maps:

$$\begin{aligned} t_\mu^{(n+1)} &= t_\mu^{(n)} + \frac{g_\mu}{D_\mu + \eta} = f_\mu(t^{(n)}, s^{(n)}) \\ s_\alpha^{(n+1)} &= s_\alpha^{(n)} + \frac{g_\alpha}{D_\alpha + \eta} = f_\alpha(t^{(n)}, s^{(n)}) \end{aligned} \quad (3)$$

Here D is a suitably chosen denominator, usually taken as the HF orbital energy difference associates with the orbital labels of μ (and α), and η is the perturbation parameter which controls the dynamics. Let vector (\tilde{t}, \tilde{s}) be the fixed points of the equation, such that $t_\mu = f_\mu(\tilde{t}, \tilde{s})$ and $s_\alpha = f_\alpha(\tilde{t}, \tilde{s})$, or in general $(t_\mu, s_\mu) = f(\tilde{t}, \tilde{s})$. Here f_μ and f_α are the functions having the same hole/particle tensor structure as g_μ and g_α respectively and f is the generic symbol of f_μ and f_α .

Following Surjan [11, 12], let's assume a small deviation around the fixed points to be ξ such that

$$(t^{(n)}, s^{(n)}) = (\tilde{t}, \tilde{s}) + \xi^{(n)} \quad (4)$$

So, employing Taylor series expansion around the fixed points, we obtain-

$$(t_\mu, s_\mu) + \xi^{(n+1)} = f(\tilde{t}, \tilde{s}) + \sum_{\nu=1}^m \left. \frac{\partial f}{\partial t_\nu} \right|_{\tilde{t}, \tilde{s}} \xi_\nu^{(n)} + \sum_{\beta=1}^m \left. \frac{\partial f}{\partial s_\beta} \right|_{\tilde{t}, \tilde{s}} \xi_\beta^{(n)} + \dots \quad (5)$$

Note from Eq. (3) that f is a function of both t_ν and s_β amplitudes. Assuming a small perturbation such that the terms $O(\xi^{(n)2})$ are negligible, one may write Eq. (5) in the long-hand notation as:

$$\xi_\mu^{(n+1)} = \sum_{\nu=1}^m \left. \frac{\partial f_\mu}{\partial t_\nu} \right|_{a,b} \xi_\nu^{(n)} + \sum_{\beta=1}^m \left. \frac{\partial f_\mu}{\partial s_\beta} \right|_{a,b} \xi_\beta^{(n)} \quad (6)$$

and

$$\xi_\alpha^{(n+1)} = \sum_{\nu=1}^m \left. \frac{\partial f_\alpha}{\partial t_\nu} \right|_{a,b} \xi_\nu^{(n)} + \sum_{\beta=1}^m \left. \frac{\partial f_\alpha}{\partial s_\beta} \right|_{a,b} \xi_\beta^{(n)} \quad (7)$$

This may be combined to write a matrix equation:

$$\begin{pmatrix} \xi_\mu^{(n+1)} \\ \xi_\alpha^{(n+1)} \end{pmatrix} = \begin{pmatrix} \frac{\partial f_\mu}{\partial t_\nu} & \frac{\partial f_\mu}{\partial s_\beta} \\ \frac{\partial f_\alpha}{\partial t_\nu} & \frac{\partial f_\alpha}{\partial s_\beta} \end{pmatrix} \begin{pmatrix} \xi_\nu^{(n)} \\ \xi_\beta^{(n)} \end{pmatrix} = J \begin{pmatrix} \xi_\nu^{(n)} \\ \xi_\beta^{(n)} \end{pmatrix} \quad (8)$$

Here J is the stability matrix. Eq. (8) forms a linearized map. The perturbed eigenvectors can be written as $\xi^{(n)} = e^{n\lambda}\xi^{(0)}$, where λ is the Lyapunov exponent. Thus, the stability matrix eigenvalue equation takes the form $J\xi^{(0)} = \sigma\xi^{(0)}$, where $\sigma = e^\lambda$ is the eigenvalue of the stability matrix and $\xi^{(0)}$ is the eigenvector.

This corresponds to a time-discrete linear state-space model which is exponentially stable if all the eigenvalues of J have a modulus smaller than one. Note that this analysis is solely based on linearization, and thus tells us nothing about the marginal cases, in which the neglected terms of the order $O(\xi^{(n)2})$ determine the local stability of the system under time-discrete propagation.

Results: The stability of the matrix depends upon its eigenvalue. If all the eigenvalues of the stability matrix are less than one (i.e., the corresponding Lyapunov exponents are negative), then the procedure converges. Thus $|\sigma| < 1$ is the convergent condition for any iterative procedure. A detailed study of the highest Lyapunov exponents of each symmetry for symmetrically stretched water (bond length = 2.6741 Bohr, bond angle = 96.774°, cc-pVDZ basis) is reported in Fig.(1). It is shown that the highest Lyapunov exponent (corresponding to A_1 symmetry) becomes positive at $\eta = 0.29$.

Near the point of equilibrium with small enough perturbation η , the system is Lyapunov stable and the iteration converges to the same set of fixed points[13]. In fact, there is a critical value of η , for which the system takes much fewer number of steps to converge. Here we quantify the effects of larger input disturbances, as done in control theory.

Around $\eta = 0.2712$, the perturbation crosses the critical value and one observes the onset of an oscillatory divergence in the initial phase of time-propagation, followed by the generation of period-2 cycle. η may be considered as a measure of the non-linearity in the system and a linear Lyapunov stability analysis is unable to predict marginal cases. For our coupled logistic map, the se-

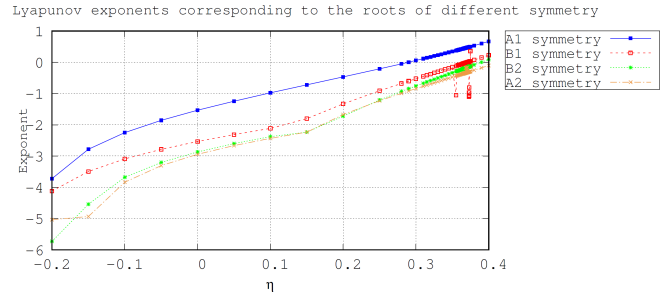


FIG. 1: Largest Lyapunov exponents corresponding to different symmetries of symmetrically stretched H_2O molecule in cc-pVDZ basis for η values from -0.2 to 0.4

vere non-linearity results in an early onset of period-2 cycles. With increasing value of the perturbation parameter, η , one further observes period- 2^n cycles ($n = 2, 3, \dots$), before the iteration becomes chaotic. Note that for such 1-dimensional dynamics, a full period doubling cascade *must* precede chaos[14]. The cluster amplitudes at an arbitrarily chosen k -th step recur at $(k + 2^n)$ -th step for period- 2^n cycle and the energy obtained by evaluating the vacuum expectation value $\langle e^{-T} W e^T \rangle$ oscillates between 2^n periods. For a range of perturbation η , it shows period-doubling bifurcation cascade (Fig. 2).

The range of the parameter for successive higher period cycles keeps on shrinking as a characteristic of the period-doubling bifurcation[15]. In fact, in the limiting case, i.e., at the onset of chaos, any single parameter map follows the dynamics such that

$$\lim_{n \rightarrow \infty} \delta \approx 4.6692, \quad \delta = \frac{\eta_{n+1} - \eta_n}{\eta_{n+2} - \eta_{n+1}} \quad (9)$$

Here η_n is the onset point of the period- 2^n cycle. The limit of δ is a universal constant, known as Feigenbaum constant. Despite being a multivariate logistic map with tensorial structure, it is indeed possible to generate all the different period cycles, as shown in Fig. 2. We have further developed a numerical algorithm based on bisection method for precise determination of the onset points of different period cycles. The first eight values of η are shown in Table I, along with the ratio δ . In the limiting case of $n \rightarrow \infty$, the δ computed shows excellent (error<0.004%) agreement to the universal value of the Feigenbaum constant. The very high value of the first ratio demonstrates an early onset of period-2 cycle, as otherwise predicted by the largest Lyapunov exponent. Thus, it tells us about the severe nonlinearity of the system. One should further note that the convergence to the exact value with higher period cycles is not monotonic, rather we observe an oscillating convergence.

Such clear separation of different periodic cycles, which is characteristic of symmetric few variable systems, indicates the presence of a set of few variables which govern the dynamics. In cases where the linear stability is lost,

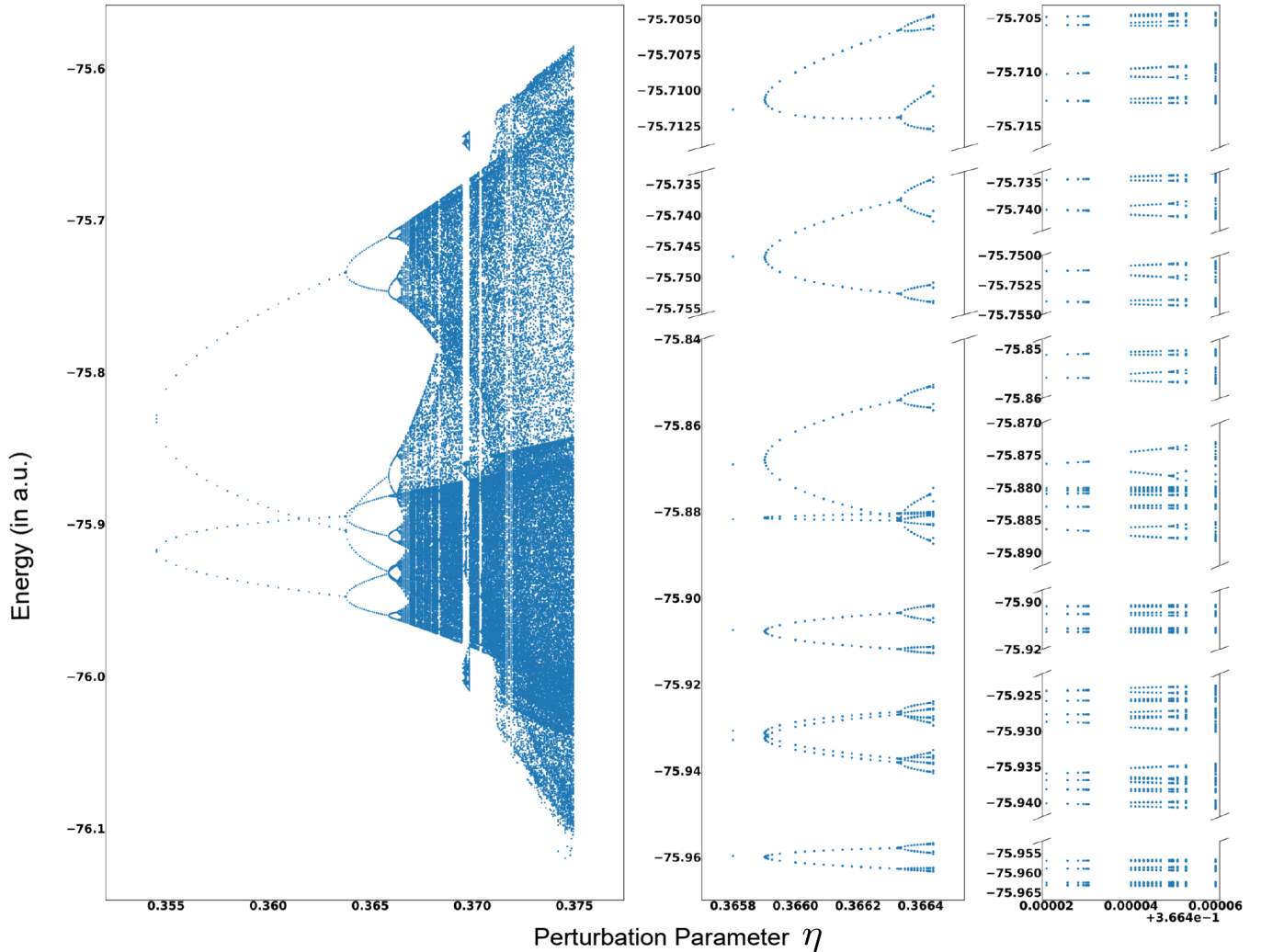


FIG. 2: The bifurcation Diagram. Magnified plots in the middle and right columns show clear presence of 16, 32, 64, 128 etc period cycles.

it is indeed possible to eliminate most of the degrees of freedom from the non-linearly interacting subsystems, so that the macroscopic behavior of the system is governed by a few degrees of freedom only [16–18]. Along this line, we presume that the dynamics of our system is dictated

n	Period ($= 2^n$)	η	δ (% error in δ)
1	2	0.2711953	–
2	4	0.3545298	–
3	8	0.363806	8.983(92.4%)
4	16	0.3659015	4.428(5.2%)
5	32	0.3663366	4.8147(3.1%)
6	64	0.36642994	4.66145(0.165%)
7	128	0.366449917	4.67237(0.068%)
8	256	0.3664541953	4.66937(0.00364%)

TABLE I: Onset points of different period cycles and Feigenbaum Constant

by *only a few* large cluster amplitudes, which are the order parameters (unstable modes) of the system that determine its macroscopic pattern.

We have further studied the dynamics with recurrence analysis[19, 20]. Here each iteration was embedded as one time step[21]. The state x_i was taken as a vector having all the values of t_2 and t_1 amplitudes at the i -th time step; $x_i = (\{t_1 \oplus t_2\}_i)^T$. Distance matrix (DM, aka unthreshold recurrence matrix), which is a useful tool to study the phase space trajectory, is defined as

$$DM_{i,j} = \|\vec{x}_i - \vec{x}_j\|, \quad i, j = 1, \dots, N \quad (10)$$

where N is the Length of time series, and $\|\cdot\|$ is a norm. Here the simulation was run for 4000 steps and plotted for the last $N = 64$ iterations.

We have plotted DM taking all the (non-zero) cluster amplitudes, here on referred as Full-T (4938 non-zero variables), and is shown for some representative η values

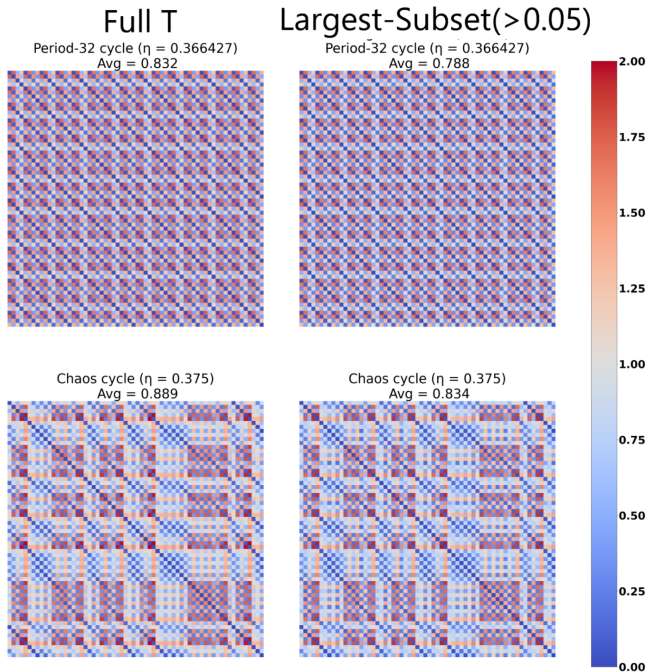


FIG. 3: Distance Matrix for a few η values with Full-T amplitudes (left column) and Largest-subset of T-amplitudes (right column). Both the horizontal and the vertical axes represent discrete time steps. The average variation calculated as $\frac{1}{N^2} \sum_{i,j} DM_{i,j}$; $N = 64$.

(Left panel of Fig. 3). To prove our hypothesis stated before, we have identified a set of few large cluster operators (total eleven) which have amplitudes >0.05 throughout the entire range of η . These operators involve at least a pair of chemically active orbitals. Henceforth we refer them as the Largest-subset. It is found that the DM for different η , constructed with the Largest-subset of amplitudes replicates the phase space trajectory to that obtained by Full-T with excellent quantitative and qualitative accuracy. This is shown in the right panel of Fig 3 at the same η values. The average variation for the largest-subset matches to that constructed with Full-T with $>93\%$ accuracy throughout the entire range of η . Thus the variation of the smaller amplitudes is almost entirely suppressed by the largest-subset, making them asymptotically negligible in the dynamics. The macroscopic pattern is solely determined by the dynamics of the large amplitudes which behave as the order parameters of the system. Their variation is independent of the microscopic sub-dynamics of the smaller amplitudes. In other words, the largest subset enslaves the smaller amplitudes. Such domination of the large amplitudes is amplified by the non-linear terms of the CC expansion, whereas the small amplitudes effectively contribute at the linear level to provide the feedback coupling.

Recurrence Quantification Analysis (RQA): Re-

currence plot (RP) is heuristic approach[22, 23] to quantify the epochs of a particular state to recur in a time-series and is based on its phase space trajectory. A recurrence matrix is defined as

$$RP_{i,j} = \Theta(\epsilon_i - DM_{i,j}) \quad (11)$$

where ϵ_i is a suitable threshold distance, and $\Theta(\cdot)$ is the Heaviside function. Thus if the $DM_{i,j}$ is less than the threshold, the corresponding $RP_{i,j} = 1$ and denoted by a black dot, otherwise $RP_{i,j} = 0$ (white dot). In RQA, one quantifies the density of recurrence points as well as the histograms of the lengths l of the diagonal based on a suitably chosen recurrence threshold. The recurrence threshold is the most significant quantity in RQA. It should be chosen small enough to distinguish the closely spaced trajectories but not small enough to miss out on the rich dynamics associated with the time series. We have chosen $\epsilon_i = 0.05$ for all further analyses.

Recurrence rate (RR), which is a measure density of RP and signifies the probability of occurrence of a specific state, is defined as

$$RR = \frac{1}{N^2} \sum_{i,j=1}^N RP_{i,j} \quad (12)$$

Thus, higher RR corresponds to a more repetitive state space trajectory. Fig. 4(a) shows the RR of our system and displays a gradual decrease from lower period cycles to higher periodic cycles and eventually to chaos. Note that the RR obtained from the time evolution of Largest-subset amplitudes (red) follows quantitatively closely to that obtained from Full-T (blue). One may note that the choice of the threshold is sensitive enough to capture chaos-period transition in the islands of stability around $\eta = 0.369$ and $\eta = 0.372$, which are characterized by sudden upward spikes in the RR plot.

Deterministic periodic systems are often characterized by repeated long and continuous diagonal lines in their RPs, signifying repeated similar state evolution. The RPs corresponding to fewer period cycles have larger number of continuous diagonal lines parallel to the Line of Identity (LOI) in a given length of the time series. Contrarily, subsequent independent values often appear as isolated single points. Thus the fraction of recurrence points appearing as diagonal points parallel to the LOI is considered to be a measure of determinism of the system:

$$DET = \frac{\sum_{l=l_{\min}}^N lP(l)}{\sum_{l=1}^N lP(l)} \quad (13)$$

, where $P(l)$ is the histogram of diagonal lines of length l . DET is a measure of predictability of the system. As a necessary (but not sufficient) condition, the periodic systems are characterized by high value of DET and this has successfully been predicted quantitatively by the RQA,

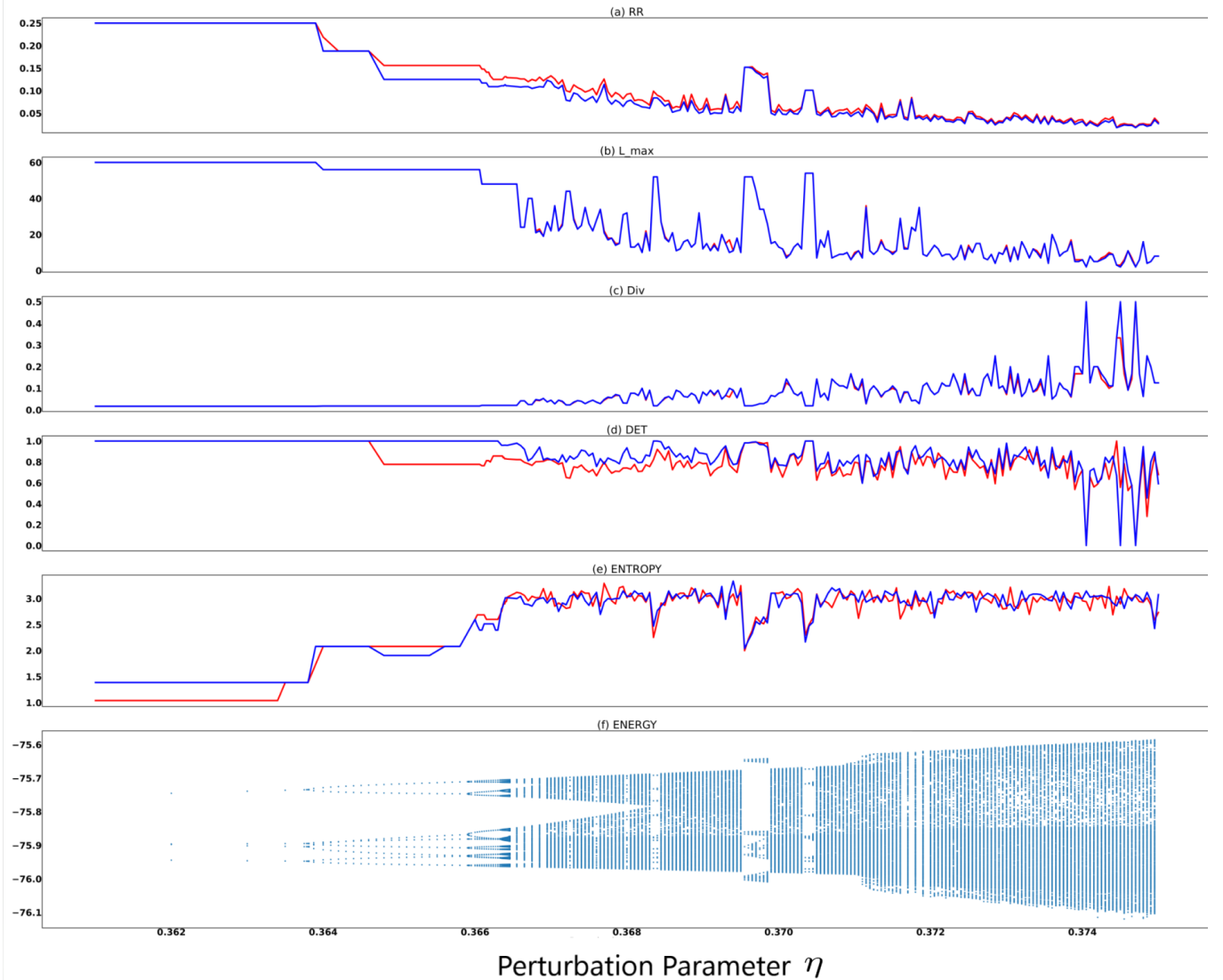


FIG. 4: Variation of RR, L_{max} , DIV, DET, and Entropy with perturbation parameter η computed via RQA. Blue line denotes the quantities with Full-T, and red line denotes that of Largest-subset. The bifurcation diagram is also presented along the same horizontal scale to identify the period-period and chaos-period transitions locations.

both with Full-T (blue) and Largest-subset (red) of T amplitudes (Fig. 4d).

High value of Maximum Diagonal Length (L_{max}), defined as $L_{max} = \max(l_i; i = 1, 2, \dots, N_l)$ is often characteristic of regular, correlated and periodic systems. In the RQA, one may roughly interpret its inverse, known as Divergence (DIV), defined as $DIV = L_{max}^{-1}$, as an estimator of Lyapunov Exponent[24]. Excluding the LOI and an appropriate Theiler window[25] around it, the other recurrence points from the subsequent phase space vectors, lead to continuous diagonal lines in the RP. Thus, the lower period cycles, with frequent recurrence of the same states, have higher L_{max} value and lower DIV. This has been quantitatively verified and shown that these two measures have identical behavior when full-T amplitudes

and Largest-subset are used (Figs. 4(b) and 4(c)).

One of the important quantities which emerges from RQA is the entropy associated with the dynamics. However, studies have shown that the using Shannon Entropy obtained from RP using its diagonal length histograms, given by $ENTR = -\sum_{l=l_{min}}^N p(l)\ln(p(l))$, where $p(l)$ is the probability distribution of the diagonal length, gives a counter-intuitive trend of entropy for period-chaos systems [26]. It is observed that such a description often show decreasing value of entropy with increasing chaos and also it anti-correlates with the maximal Lyapunov exponent. A number of methods have been suggested for calculation of entropy[26–28]. Following Eroglu *et al.*[28], we have calculated it from Weighted Distance Ma-

trix(WDM), defined by

$$W_{i,j} = e^{-\|x_i - x_j\|} \quad (14)$$

For entropy calculation, we define strength (s_i) as $s_i = \sum_{j=1}^N W_{i,j}$. The strength is used to calculate Shannon Entropy associated with the WDM through the distribution of $P(s)$.

$$ENTR = - \sum_{\{s\}} p(s) \ln p(s) \quad (15)$$

where $p(s) = P(s)/S$ is the relative frequency distribution of WDM and $S = \sum_i^N s_i$. The variation of $ENTR$ with respect to η is shown in Fig. 4(e). Clearly this correlates with the Lyapunov exponent and shows all the jumps and dips of period-period and chaos-period transitions across different range of η . The $ENTR$ predicted with the Full-T amplitudes and that with the largest subset follow closely throughout, thus $ENTR$ is shown to be governed solely by the active excitations. All such RQA measures are found to be largely independent of the time-series embedding dimension.

Conclusion: In summary, we have shown, for the first time, that the discrete-time propagation of a double similarity transformed CC theory shows the dynamical features of a logistic map. The universality of the dynamics is confirmed by computing accurate value of the Feigenbaum constant. Further to that, recurrence analysis was performed with the state vectors comprising all the cluster amplitudes and that with the largest subset thereof. The RQA shows identical phase space trajectory for these two cases. This reinforces our hypothesis of a master-slave dynamics.

Acknowledgement: RM acknowledges IIT Bombay Seed grant, and Science and Engineering Research Board, Government of India, for financial support. Discussions with Professors Debashis Mukherjee and Sandip Kar are acknowledged.

* rmaitra@chem.iitb.ac.in

[1] J. Čížek, J. Chem. Phys. **45**, 4256 (1966).
 [2] J. Čížek, Adv. Chem. Phys. **14**, 35 (1969).

[3] J. Čížek and J. Paldus, Int. J. Quantum Chem. **5**, 359 (1971).
 [4] R. J. Bartlett and M. Musial, Rev. Mod. Phys. **79**, 291 (2007).
 [5] J. D. Watts, J. Gauss, and R. J. Bartlett, J. Chem. Phys. **98**, 8718 (1993).
 [6] K. Ragavachari, G. W. Trucks, J. A. Pople, and M. Head-Gordon, Chem. Phys. Lett. **157**, 479 (1989).
 [7] R. J. Bartlett, J. D. Watts, S. A. Kucharski, and J. Noga, Chem. Phys. Lett. **165**, 513 (1990).
 [8] R. Maitra, Y. Akinaga, and T. Nakajima, J. Chem. Phys. **147**, 074103 (2017).
 [9] R. Maitra and T. Nakajima, J. Chem. Phys. **147**, 204108 (2017).
 [10] M. Nooijen and V. Lotrich, J. Chem. Phys. **113**, 4549 (2000).
 [11] P. Szakács and P. R. Surján, Int. J. Quantum Chem. **108**, 2043 (2008).
 [12] P. Szakács and P. R. Surján, J. Math. Chem. **43**, 314 (2008).
 [13] I. Malkin, *Theory of Stability of Motion, Chap. II* (State Publishing House, Moscow-Leningrad, 1952).
 [14] J. A. Yorke and K. T. Alligood, Comm. Math. Phys. **101**, 305 (1985).
 [15] M. J. Feigenbaum, J. Stat. Phys. **19**, 25 (1978).
 [16] H. Haken, “Nonlinear equations. the slaving principle,” in *Advanced Synergetics: Instability Hierarchies of Self-Organizing Systems and Devices* (Springer Berlin Heidelberg, Berlin, Heidelberg, 1983) pp. 187–221.
 [17] H. Haken and A. Wunderlin, Z. Phys. B **47**, 179 (1982).
 [18] H. Haken, Rep. Prog. Phys. **52**, 515 (1989).
 [19] H. Poincaré, Acta mathematica **13**, A3 (1890).
 [20] J.-P. Eckmann, S. Kamphorts, and D. Ruelle, Europhys. Lett. **4**, 937 (1987).
 [21] J. P. Zbilut and C. L. Webber Jr, Phys. Rev. A **171**, 199 (1992).
 [22] N. Marwan, M. C. Romano, M. Thiel, and J. Kurths, Phys. Rep. **438**, 237 (2007).
 [23] N. Marwan, M. C. Romano, M. Thiel, and J. Kurths, “www.recurrence-plot.tk recurrence plots,” (accessed May 19, 2020).
 [24] L. Trulla, A. Giuliani, J. Zbilut, and C. Webber Jr, Phys. Rev. A **223**, 255 (1996).
 [25] J. Theiler, J. Opt. Soc. Am. A **7**, 1055 (1990).
 [26] C. Letellier, Phys. Rev. Lett. **96**, 254102 (2006).
 [27] G. Corso, T. d. L. Prado, G. Z. d. S. Lima, J. Kurths, and S. R. Lopes, Chaos: An Interdisciplinary Journal of Nonlinear Science **28**, 083108 (2018).
 [28] D. Eroglu, T. K. DM. Peron, N. Marwan, F. A. Rodrigues, L. d. F. Costa, M. Sebek, I. Z. Kiss, and J. Kurths, Phys. Rev. E **90**, 042919 (2014).